HHS Public Access

Author manuscript

ACS Infect Dis. Author manuscript; available in PMC 2020 December 13.

Published in final edited form as:

ACS Infect Dis. 2019 December 13; 5(12): 1996–2002. doi:10.1021/acsinfecdis.9b00207.

Radiosynthesis and PET Bioimaging of ^{76}Br-Bedaquiline in a Murine Model of Tuberculosis

Alvaro A. Ordonez[1,2,3,*], **Laurence S. Carroll**[4,*], **Sudhanshu Abhishek**[1,2,3], **Filipa Mota**[1,2,3], **Camilo A. Ruiz-Bedoya**[1,2,3], **Mariah H. Klunk**[1,2,3], **Alok K. Singh**[1,2,3], **Joel S. Freundlich**[5], **Ronnie C. Mease**[4], **Sanjay K. Jain**[1,2,3,4,#]

[1]Center for Tuberculosis Research, Johns Hopkins University School of Medicine, Baltimore, Maryland, USA. [2]Center for Infection and Inflammation Imaging Research, Johns Hopkins University School of Medicine, Baltimore, Maryland, USA. [3]Department of Pediatrics, Johns Hopkins University School of Medicine, Baltimore, Maryland, USA. [4]Russell H. Morgan Department of Radiology and Radiological Science, Johns Hopkins University School of Medicine, Baltimore, Maryland, USA. [5]Department of Pharmacology, Physiology, and Neuroscience, Rutgers University - New Jersey Medical School, Newark, NJ, USA.

Abstract

Bedaquiline is a promising drug against tuberculosis (TB), but limited data are available on its intralesional pharmacokinetics. Moreover, current techniques rely on invasive tissue resection, which is difficult in humans and generally limited even in animals. In this study, we developed a novel radiosynthesis for ^{76}Br-bedaquiline and performed noninvasive, longitudinal whole-body positron emission tomography (PET) in live, *Mycobacterium tuberculosis*-infected mice over 48 hours. After the intravenous injection, ^{76}Br-bedaquiline distributed to all organs and selectively localized to adipose tissue and liver, with excellent penetration into infected lung lesions (86%) and measurable penetration into the brain parenchyma (15%). *Ex vivo* high resolution, two-dimensional autoradiography and same section hematoxylin / eosin and immunofluorescence provided detailed intralesional drug biodistribution. PET bioimaging and high-resolution autoradiography are novel techniques that can provide detailed, multi-compartment and intralesional pharmacokinetics of new and existing TB drugs. These technologies can significantly advance efforts to optimize drug dosing.

Graphical Abstract

[#]Corresponding author: Sanjay K. Jain, 1550 Orleans Street, CRB-II Room 1.09, Baltimore, MD, 21287, USA, sjain5@jhmi.edu, Phone: 410-502-8241, Fax: 410-614-8173.

Author contributions. A.A.O. and L.S.C. contributed equally to this work. A.A.O. and S.K.J. conceptualized the project. L.S.C. and F.M. developed the chemical synthesis and performed the radiolabeling and validation experiments. A.A.O., C.A.R-B. and M.H.K. performed animal experiments. A.A.O., C.A.R-B. analyzed the PET data and performed statistical analysis. S.A. and A.K.S performed histology and autoradiography. R.C.M. and J.S.F. provided technical expertise on the chemical syntheses. S.K.J. supervised this project and provided funding. A.A.O. and L.S.C wrote the initial draft and all co-authors edited and approved the manuscript.

[*]Co-first authors

Notes: The authors declare no competing financial or other interests.

Supplementary information: Please refer to the supplementary data for information not reported in the main manuscript.

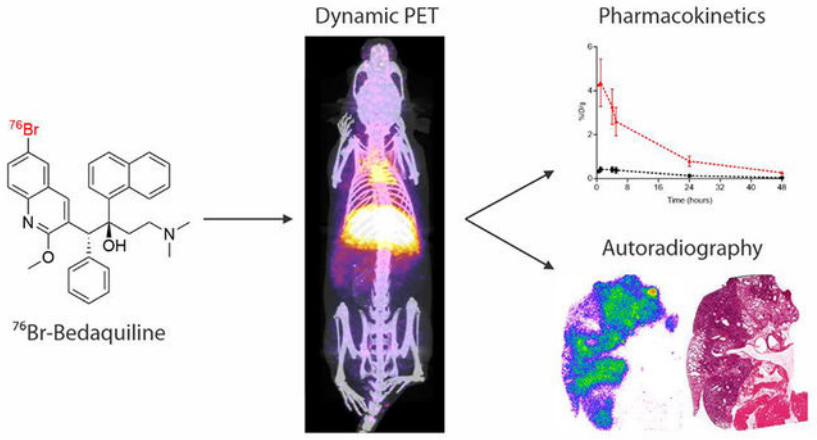

Keywords

PET; pharmacokinetics; pulmonary; TB meningitis; autoradiography

Dosing recommendations for antibiotics were developed based on plasma levels and historic measures of efficacy. While plasma pharmacokinetics (PK) are considered essential in the developmental pipeline for new antibiotics, they do not always correlate with intralesional PK. This is due to the differential partitioning of certain drugs into tissues from the plasma compartment and dependent on both the drug characteristics and host factors including lesion pathology. Due to the difficulties of direct sampling of infected tissues, data on intralesional drug concentrations at the sites of infection (where bacteria reside) are often not established, hindering the PK modeling efforts to optimize antibiotic treatments.[1] Inappropriate antibiotic levels within these target tissues can lead to treatment failure, selection of resistant organisms, and toxicity. Reduced penetration of the drugs into privileged sites can also lead to the poor performance of the drug-containing treatment regimen in the follow up complex and expensive clinical trials. Therefore, detailed data on intralesional PK at infection sites could support PK modeling and substantially boost optimization of TB treatments.

Bedaquiline, a bromine-containing diarylquinoline, is the first of a new class of anti-tuberculosis (TB) compounds that inhibit the mycobacterial ATP synthase, with a high *in vitro* activity against drug-susceptible and resistant *Mycobacterium tuberculosis*.[2] Bedaquiline was approved under the accelerated U.S. FDA program for treatment of multi-drug resistant (MDR) TB.[3] It offers synergy with both first- and second-line TB drugs and also activity against non-tuberculous mycobacteria (NTM).[4] Bedaquiline, in combination with a second-line antibiotic regimen, was found to significantly reduce the time needed for sputum conversion amongst MDR-TB patients.[5–6] The bactericidal activity of bedaquiline is concentration dependent and the area under the curve (AUC) is the main driver for dose optimization.[7] For MDR-TB patients, the recommended dosage of bedaquiline is 400 mg once daily for two weeks followed by 200 mg three times per week (with at least 48 hours between doses). While bedaquiline is a highly promising drug, the biodistribution of bedaquiline in *M. tuberculosis*-infected tissues and privileged compartments (e.g.,

pulmonary cavities, brain) remains poorly studied. Bedaquiline has been shown to have reduced penetration into caseous necrotic granulomas in mice using post-mortem analyses.[8] Similarly, the biodistribution of bedaquiline into other target organs is limited and only available via post-mortem analyses.[9] This is relevant as bedaquiline can also cause side effects (e.g., prolongation of the QT-interval, which is a measurement made on an electrocardiogram from the start of the Q wave to the end of the T wave and used to assess the electrical properties of the heart) leading to safety warnings by regulatory agencies.[3, 10] Therefore, information on intralesional levels of bedaquiline in infected tissues, as well as other target organs, is necessary to accurately optimize dosing without increasing toxicity.

Positron emission tomography (PET) is a clinically translatable molecular imaging technique that can noninvasively provide whole-body biodistribution and pharmacokinetics (PK) of radiolabeled drugs with high sensitivity (nano- to picomolar concentrations),[11] and also allow longitudinal measurements of the same subject at multiple time points. The PET signal can be then quantified to establish the concentration of the drug in different organs, particularly at the site(s) of infection.[12] Here we report a novel radiosynthesis of bromine-76-labeled bedaquiline (^{76}Br-bedaquiline), which is chemically identical to the parent drug, and its biodistribution using PET bioimaging in a murine model of pulmonary TB that develops necrotic and hypoxic TB granulomas after aerosol infection with *M. tuberculosis*.[13–15] In addition, we also report detailed, intralesional distribution of ^{76}Br-bedaquiline by utilizing high resolution, two-dimensional (2D)-autoradiography. Since autoradiography is non-destructive, the same tissue sections were also probed using immunofluorescence and hematoxylin and eosin stain to provide accurate co-localization of drug biodistribution.

Results and Discussion

Radiosynthesis of ^{76}Br-Bedaquiline

The positron emitter isotope bromine-76 was introduced into bedaquiline by replacing the endogenous bromine and therefore ^{76}Br-bedaquiline is chemically identical to the parent drug. Since the physical (radiological) half-life of bromine-76 is 16.2 hours, whole-body PET can be performed at multiple time-points over 48 hours. The position of the radiolabel was chosen to ensure that it would be retained on the molecule even if the drug were metabolized to the the *N*-monodes-methyl metabolite (M2).[16] Radiosynthesis of an isotopic analog of the parent compound, bedaquiline **1** was achieved *via* a boronic ester precursor **2** and a copper catalyst to produce **[^{76}Br]1**.[17–18] Non-isotopically labeled bedaquiline was reacted with bis(pinacolato)diboron and [1,1′-bis(diphenylphosphino)ferrocene]dichloropalladium(II), giving a 60 ± 5 % (n = 3) conversion to the desired boronic ester **2** (Figure 1).[19] This mixture was subsequently purified *via* a combination of flash column chromatography and semi-preparative HPLC to provide pure precursor for our labeling experiments, confirmed using both NMR and LCMS.

^{76}Br-Bedaquiline (**[^{76}Br]1**) was synthesized by reacting precursor **2** with $NH_4{}^{76}Br$ (Figure 1). Briefly, aqueous bromide-76 was neutralized with ammonium hydroxide (20 μl), concentrated to ~100 μl, precursor **2** in DMSO was added, and the mixture heated at 100°C to provide 20% conversion, observed by HPLC after 20 min. ^{76}Br-Bedaquiline was isolated

by preparative HPLC in a 6% non-decay corrected radiochemical yield (n=5) (Supplementary Figure 1). The identity of the labeled compound was confirmed by co-injection of standard bedaquiline and the synthesized **[^{76}Br]1** using analytical HPLC.

^{76}Br-Bedaquiline PET bioimaging

It is increasingly being recognized that heterogeneous pathological states - cavitation, pneumonia, and necrotic granulomas - occur simultaneously within the same pulmonary TB patient,[20] each with a distinct bacterial burden and antibiotic exposure, which are dynamic.[12] Easily available clinical samples [e.g., blood, cerebrospinal fluid (CSF)] fail to capture the complex and dynamic nature of heterogeneous TB lesions or pathological states that may occur simultaneously within the same subject.[12] Similarly, while advanced techniques [e.g., matrix-assisted laser desorption ionization (MALDI)] can detect drugs and their metabolites in infected tissues, they are invasive, rely on accurate resection of tissues,[8] and introduce sampling bias (given the multiple, heterogeneous lesions in the same host) or artifacts introduced during animal sacrifice / tissue processing. Moreover, tissue resection is difficult in humans and generally limited to a single time-point even in animals. Therefore, longitudinal assessments to measure antibiotic penetration over time with current tools, are difficult even in animal models, and current tools also have limited translational potential for use in clinical studies.

To determine the *in vivo* biodistribution of ^{76}Br-bedaquiline, we utilized a mouse model that develops necrotic pulmonary granulomas after aerosol infection with *M. tuberculosis*. Similar to humans, these animals develop a heterogeneous pulmonary disease that includes granulomas, pneumonia areas, and cavities.[15] Ten weeks after aerosol infection with *M. tuberculosis*, the animals had a pulmonary bacterial burden of 8.06 ± 0.68 $\log_{10}$ colony forming units (CFU). Whole-body PET was performed at multiple time-points in the same cohort of live animals over 48 hours (Figure 2). Multiple regions of interest (ROI) were drawn and the ^{76}Br-bedaquiline signal was measured at each time-point in several organs as well as infected and unaffected pulmonary tissues to obtain time-activity curves and AUCs over 48 hours (AUC_{48h}). Overall, 283 different measurements were made over 48 hours, of which 81 were from the infected lung tissues.

Since plasma PK for bedaquiline after oral dosing are already established in animals and humans,[7, 21] the primary goal of our current study was to establish AUC tissue/plasma ratios ($AUC_{tissue/plasma}$) using PET, which in conjunction with plasma PK, would allow us to accurately measure intralesional bedaquiline concentrations. Intravenous injection of ^{76}Br-bedaquiline (rather than oral administration) was therefore utilized for these studies. Intravenous dosing generally leads to more reliable plasma PK and is utilized extensively in PET studies for establishing drug PK.[22] We have recently described these PET imaging methods to measure tissue concentrations of rifampin in difficult to sample and privileged compartments in animal models of TB and patients with active TB.[12] After intravenous injection, ^{76}Br-bedaquiline distributed to all parts of the body and selectively localized to adipose tissue (brown fat) and liver (Figure 2A, B). Penetration into infected lung lesions was high with an $AUC_{tissue/plasma}$ ratio of 86.29 ± 13.62% (Figure 2C and Supplementary Figure 2). High-resolution PET also allowed a detailed characterization of the

biodistribution of ^{76}Br-bedaquiline in all the lung regions at several time-points (Supplementary Figure 3). ^{76}Br-Bedaquiline distribution was spatially heterogeneous but penetration was noted into infected pulmonary tissues during the 48 hours observed (Supplementary Figure 4). It should be noted that we measured AUC during the first 48 hours while Irwin *et al.* reported the AUC up to 168 hours after oral dosing.[8] In addition, while PET cannot differentiate between bedaquiline and M2, PET signal from the tissues measures both the parent drug and M2, which is also active against *M. tuberculosis* and thus therapeutically relevant.

Since PET can simultaneously sample multiple compartments and organs, we were also able to measure drug penetration into several different compartments. For example, there was limited but measurable penetration of ^{76}Br-bedaquiline into the brain parenchyma with an $AUC_{tissue/plasma}$ ratio of 14.81 ± 2.12% (Figure 2D and Supplementary Figure 2). TB meningitis is a serious and often fatal form of TB and disproportionately affecting vulnerable populations - young children and HIV-infected individuals.[23] Treatments developed ~50 years ago prevent death or disability in less than half of those afflicted by this disease.[24] Moreover, several key antimicrobials have limited penetration into the central nervous system (including the brain parenchyma) and the lack of PK data for existing and new TB drugs is a significant challenge, especially given the alarming rise of MDR-TB.[25–26] We therefore believe that penetration of ^{76}Br-bedaquiline into the brain parenchyma is a novel finding as the concentration of bedaquiline in brain tissues of *M. tuberculosis*-infected animals has not been reported previously. While Pamreddy *et al.* have reported the penetration of bedaquiline (35% of administered oral dose) in healthy rats using MALDI,[9] a case report describing a 36-year old patient with TB meningitis, demonstrated no detectable levels of bedaquiline in the CSF obtained through an external lumbar drainage at ~6 and 11 weeks after initiation of bedaquiline and TB treatment respectively.[27] There could be several reasons for this discrepancy, including limited penetration of bedaquiline into the CSF, possibly due to decreased inflammation and permeability of the blood-CSF barrier several weeks after the initiation of treatment.[12] Importantly, different partitioning of bedaquiline (which is highly lipophilic and protein-bound) preferentially into the brain parenchyma (measured in the current study) rather than CSF which is hydrophilic, may also explain these findings. In addition, Rohlwink *et al.* have demonstrated that biochemical characteristics of lumbar CSF are different from that obtained from the ventricles in patients with TB meningitis,[28] potentially due to barriers which may affect the uniform circulation of CSF, reinforcing the need for measuring drug concentrations at the infection site. Additional studies in relevant animal models[12] are needed to answer these questions. The biodistribution of ^{76}Br-bedaquiline into kidneys, bladder, spleen, muscle, brown fat and bone is shown in Supplementary Figure 5.

Some animals were also sacrificed for post-mortem, high-resolution 2D-autoradiography to measure detailed, intralesional distribution of ^{76}Br-bedaquiline (Figure 3A). Autoradiography utilizes an X-ray film to detect radioactive materials and produces a permanent record of the positions and relative intensities of the radiolabeled source.[29] At an early time-point (6 hours after tracer-injection), ^{76}Br-bedaquiline signal was reduced in infected versus unaffected areas with diffuse distribution in pneumonic areas and consistent with the PET data obtained in live animals at the same time-point after tracer-injection

(Supplementary Figure 4). Unlike techniques such as MALDI, autoradiography is non-destructive. Therefore, the same tissue sections were also probed using immunofluorescence and H&E staining to demonstrate the localization of CD68+ cells and bacteria in the same sections (Figure 3B, C and Supplementary Figure 6).

In summary, we report a novel technique to noninvasively study whole-body biodistribution of bedaquiline using PET. Moreover, we also demonstrate proof-of-principle and feasibility of high-resolution, 2D-autoradiography to measure detailed, intralesional distribution of ^{76}Br-bedaquiline. Given that the same section can be used to obtain high-resolution spatial localization of the drug (autoradiography), as well as perform additional stains for inflammatory cell types, bacteria, cellular targets, etc., this technology would allow for accurate co-localization studies in 2 and 3-dimensions. PET bioimaging has several advantages over current methods and provides holistic three-dimensional information to simultaneously evaluate heterogeneous lesions in multiple compartments and thus limit sampling bias. Importantly, as demonstrated, longitudinal profiling in the same subjects at several time-points can be performed thereby reducing animal-to-animal variability and costs associated with sacrificing different animal cohorts at each time-point. PET can provide rapid (same day) *in situ* measurements in live (infected) subjects with intact physiology and without artifacts (due to animal sacrifice / processing). In the future, this technology could be utilized for studies in larger and more expensive animal models of TB (e.g., rabbits, non-human primates) as well as for other infectious pathogens such as NTM and *Staphylococcus aureus*, which have similar challenges and where bedaquiline is also being used to treat MDR infections. Finally, since PET is fully translatable to the clinic,[12] this technology will also allow clinical assessments, especially early proof-of-concept studies which typically require 10–20 patients, and are highly encouraged by the U.S. FDA.

Materials and Methods

All protocols were approved by the Johns Hopkins Biosafety, Radiation Safety, and Animal Care and Use Committees.

General Materials and Methods:

Chemicals and solvents were purchased from CarboSynth, Sigma-Aldrich, and TCI America and were used as received. Anhydrous solvents (glacial acetic acid, dioxane, acetonitrile, THF, and toluene) were purchased from Aldrich. EtOAc, petroleum ether and hexanes were purchased from Fisher Scientific. Unless stated, reactions were performed under an inert atmosphere of dry argon gas (Ar) in oven-dried (150 °C) glassware.

Synthesis of Boronic Ester 2:

Bedaquiline **1** (100 mg, 0.180 mmol) was dissolved in dioxane (4 ml) and to it B_2pin_2 (43.2 mg, 0.170 mmol), $Pd(dppf)_2Cl_2$ (3.7 mg, 0.005 mmol) and KOAc (50.4 mg, 0.514 mmol) was added. The reaction mixture was heated to 80 °C for 16 hours, and then cooled to room temperature and diluted with DCM (~15 ml). The subsequent heterogeneous solution was filtered through Celite® and the resultant filtrate was concentrated *in vacuo*. The residue was purified *via* flash column chromatography (silica, 100% EtOAc), before subsequent

purification using semi-preparative HPLC, which was performed using a Phenomenex Luna C18(2) 10 μm, 250 × 4.6 mm column, at a flow rate of 10 mL/min, using water and acetonitrile containing 0.1 % TFA as the mobile phases. The following gradient was applied: 40 % acetonitrile for 2 min, 40 – 100 % over 10 min, 100 % for 3 min, and 100 – 40 % over 2 min. The boronic ester eluted between 8.2 and 8.6 min. Upon evaporation of the solvent the precursor was dried under vacuum overnight and a white powder was obtained. ^{1}H NMR (500 MHz, DMSO-d_6) δ 9.10 (s, 1H), 8.85 (s, 1H), 8.64 (s, 1H), 8.35 (s, 1H), 7.94 (s, 1H), 7.87 (d, J = 8.3 Hz, 1H), 7.74 (d, J = 8.4 Hz, 3H), 7.56 (s, 1H), 7.32 (t, J = 7.8 Hz, 1H), 7.12 (s, 2H), 6.90 (s, 3H), 5.77 (s, 2H), 4.22 (s, 3H), 3.05 (d, J = 63.2 Hz, 2H), 2.46 (s, 2H), 1.35 (s, 12H), 1.18 (s, 6H). ^{13}C NMR (126 MHz, DMSO) δ 156.4 (qC), 140.7 (qC), 139.3 (qC), 136.6 (CH), 135.5(CH), 134.3 (CH), 130.3 (CH), 130.2 (CH), 129.0 (CH), 127.8 (CH), 127.77 (CH), 126.4 (CH), 126.2 (CH), 125.6 (qC), 125.5 (CH), 125.0 (CH), 115.3 (qC), 84.7 (qC), 83.3 (qC), 54.7 (CH_2), 43.3 (CH_3), 42.46 (CH_3), 34.8 (CH_2) 25.81 (CH_3). LRMS (ESI $^{+}$) $[M+H]^{+}$ Calculated for $C_{38}H_{44}BN_2O_4]^{+}$: 603.3; Found: 602.9.

[^{76}Br]Bromide:

^{76}Br was produced at the Washington University School of Medicine using a CS-15 Cyclotron (Cyclotron Corporation). Briefly, a $^{63}Cu_2{}^{76}Se$ disc was bombarded with protons (15 MeV beam, 5–20 μA) and the resultant ^{76}Br was separated using thermal distillation. ^{76}Br was collected in a basic solution and purified using a Sep-Pak C-18 cartridge.

Synthesis of ^{76}Br-Bedaquiline:

Aqueous [^{76}Br]bromide (500 μl, up to 370 MBq) was added to NH_4OH (28% in H_2O, 10 μl) and dried at 100 °C in a Wheaton vial with a constant stream of N_2. Within approximately 10 minutes, the total volume of the solution had reduced to 50–100 μl, and this was used directly for radiolabeling experiments without further purification. Boronic ester **2** (3 mg) was dissolved in DMSO (400 μL) with $Cu(OTf)_2(Py)_4$ (2 mg) inside a Wheaton vial, and to this mixture was added the concentrated bromide solution (50 μl, up to 370 MBq). The reaction was heated at 100 °C for 10 minutes, before being cooled to approximately 30 °C. The reaction mixture was diluted with water (10 ml) and purified by semi-preparative HPLC, which was performed using a Phenomenex Luna C18(2) 10 μm, 250 × 4.6 mm column, at a flow rate of 2 mL/min, using water and acetonitrile as the mobile phases. The following gradient was applied: 5 % acetonitrile for 5 min, 5 – 95 % over 20 min, 95 % for 5 min, 95 – 5 % over 5 min, and 5 % for 5 min. ^{76}Br-Bedaquiline eluted at 25 min. The desired compound **[^{76}Br]1**, was diluted with PBS (100 μl) and concentrated at 80 °C with a constant stream of N_2 affording the final formulated product in a 6 ± 1 % n.d.c. radiochemical yield (18–24 MBq, n = 5).

Animal infection:

Four to six-week-old female C3HeB/FeJ mice (Jackson Laboratory) were aerosol-infected with frozen stocks of *M. tuberculosis* (H37Rv), using the Middlebrook Inhalation Exposure System (Glas-Col) as described previously.[30] Ten weeks after infection, a separate group of three animals was sacrificed with their lungs harvested to determine the bacterial burden. Lung homogenates in serial dilutions were plated on 7H11 agar plates.

PET Imaging:

After an incubation period of 10 weeks post-infection, *M. tuberculosis*-infected animals were injected with 1.30 ± 0.12 MBq of ^{76}Br-bedaquiline via tail vein and imaged within a sealed bio-containment bed (Minerve), as described previously.[15] Computed tomography (CT) and PET were performed using the nanoScan PET/CT (Mediso) with 30 min acquisition frames at 30 min, 1, 4, 5, 24 and 48 hours post injection of the tracer. Scatter and attenuation correction was applied to the images and were analyzed using VivoQuant 3.0 (Invicro) for visualization. Quantification of the biodistribution of the radiolabeled drug was performed by drawing ROI, based on the CT, for quantification using AMIDE 1.0.4. For each lesion, the ROIs were drawn in the same region for each time-point to quantify the same lesion over 48 hours. Data for blood activities were obtained by placing an ROI in the left ventricle of the heart and converted to plasma using the hematocrit.[31] The PET data were adjusted for mass using the density of each ROI (obtained from the CT as Hounsfield units) and are expressed as % injected dose (ID) / weight (g).

Autoradiography:

3.0 MBq of ^{76}Br-bedaquiline were injected via tail vein to an *M. tuberculosis*-infected mouse which was sacrificed by isoflurane overdose three hours later for autoradiography. The lungs were harvested, fixed in optimal cutting temperature compound (OCT) and sliced using a Cryostat CM1950 (Leica Microsystems) into multiple 20 μm sections. The frozen lung sections were exposed overnight to high-performance autoradiography X-ray film (Biomax) and were developed using standard photographic methods in a dark room within the biosafety level (BSL)-3 facility. The spatial biodistribution of ^{76}Br-bedaquiline in the X-ray film was determined using a high-resolution flatbed scanner and densitometry software MCID Elite image analysis Version 7.0 (Imaging Research Inc.).

Immunofluorescence and Histopathology:

After autoradiographs were developed, the same tissue section was fixed in 4% paraformaldehyde in PBS and stained using immunofluorescence techniques. Macrophages were probed with anti-CD68 [FA-11]-Alexa Flour 647 (Abcam 201845), the mycobacteria were probed with anti-*M. tuberculosis*-FITC (Abcam 20962) and the nuclei were stained with DAPI at room temperature. The tissue sections were mounted with ProLong Gold Antifade (ThermoFisher Scientific) and visualized under laser scanning confocal microscope (Leica Microsystems) with DAPI, FITC, and Cy5 filters. These sections were subsequently stained with hematoxylin and eosin.

Statistical analysis:

Data was analyzed using Prism 8 version 8.1.0 (GraphPad). AUCs were calculated using the linear trapezoidal rule. Comparisons were made using a two-tailed, Mann Whitney *U* test. *P* values less than 0.05 were considered statistically significant.

Supplementary Material

Refer to Web version on PubMed Central for supplementary material.

Funding:

NIH Director's Transformative Research Award R01-EB020539 (SKJ), and NIH R56-AI145435 (SKJ).

References

1. Reynolds J; Heysell SK, Understanding pharmacokinetics to improve tuberculosis treatment outcome. Expert Opin Drug Metab Toxicol 2014, 10 (6), 813–23. [PubMed: 24597717]
2. Andries K; Verhasselt P; Guillemont J; Göhlmann HW; Neefs J-M; Winkler H; Van Gestel J; Timmerman P; Zhu M; Lee E, A diarylquinoline drug active on the ATP synthase of Mycobacterium tuberculosis. Science 2005, 307 (5707), 223–227. [PubMed: 15591164]
3. Cox E; Laessig K, FDA approval of bedaquiline--the benefit-risk balance for drug-resistant tuberculosis. N Engl J Med 2014, 371 (8), 689–91. [PubMed: 25140952]
4. van Heeswijk RP; Dannemann B; Hoetelmans RM, Bedaquiline: a review of human pharmacokinetics and drug-drug interactions. The Journal of antimicrobial chemotherapy 2014, 69 (9), 2310–8. [PubMed: 24860154]
5. Diacon AH; Donald PR; Pym A; Grobusch M; Patientia RF; Mahanyele R; Bantubani N; Narasimooloo R; De Marez T; van Heeswijk R; Lounis N; Meyvisch P; Andries K; McNeeley DF, Randomized pilot trial of eight weeks of bedaquiline (TMC207) treatment for multidrug-resistant tuberculosis: long-term outcome, tolerability, and effect on emergence of drug resistance. Antimicrob Agents Chemother 2012, 56 (6), 3271–6. [PubMed: 22391540]
6. Diacon AH; Pym A; Grobusch MP; de los Rios JM; Gotuzzo E; Vasilyeva I; Leimane V; Andries K; Bakare N; De Marez T; Haxaire-Theeuwes M; Lounis N; Meyvisch P; De Paepe E; van Heeswijk RP; Dannemann B; Group TCS, Multidrug-resistant tuberculosis and culture conversion with bedaquiline. N Engl J Med 2014, 371 (8), 723–32. [PubMed: 25140958]
7. Rouan MC; Lounis N; Gevers T; Dillen L; Gilissen R; Raoof A; Andries K, Pharmacokinetics and pharmacodynamics of TMC207 and its N-desmethyl metabolite in a murine model of tuberculosis. Antimicrob Agents Chemother 2012, 56 (3), 1444–51. [PubMed: 22155815]
8. Irwin SM; Prideaux B; Lyon ER; Zimmerman MD; Brooks EJ; Schrupp CA; Chen C; Reichlen MJ; Asay BC; Voskuil MI; Nuermberger EL; Andries K; Lyons MA; Dartois V; Lenaerts AJ, Bedaquiline and Pyrazinamide Treatment Responses Are Affected by Pulmonary Lesion Heterogeneity in Mycobacterium tuberculosis Infected C3HeB/FeJ Mice. ACS Infect Dis 2016, 2 (4), 251–267. [PubMed: 27227164]
9. Pamreddy A; Baijnath S; Naicker T; Ntshangase S; Mdanda S; Lubanyana H; Kruger HG; Govender T, Bedaquiline has potential for targeting tuberculosis reservoirs in the central nervous system. RSC Advances 2018, 8 (22), 11902–11907.
10. Fox GJ; Menzies D, A Review of the Evidence for Using Bedaquiline (TMC207) to Treat Multi-Drug Resistant Tuberculosis. Infect Dis Ther 2013, 2 (2), 123–44. [PubMed: 25134476]
11. James ML; Gambhir SS, A molecular imaging primer: modalities, imaging agents, and applications. Physiol Rev 2012, 92 (2), 897–965. [PubMed: 22535898]
12. Tucker EW; Guglieri-Lopez B; Ordonez AA; Ritchie B; Klunk MH; Sharma R; Chang YS; Sanchez-Bautista J; Frey S; Lodge MA; Rowe SP; Holt DP; Gobburu JVS; Peloquin CA; Mathews WB; Dannals RF; Pardo CA; Kannan S; Ivaturi VD; Jain SK, Noninvasive (11)C-rifampin positron emission tomography reveals drug biodistribution in tuberculous meningitis. Sci Transl Med 2018, 10 (470).
13. Pan H; Yan BS; Rojas M; Shebzukhov YV; Zhou H; Kobzik L; Higgins DE; Daly MJ; Bloom BR; Kramnik I, Ipr1 gene mediates innate immunity to tuberculosis. Nature 2005, 434 (7034), 767–72. [PubMed: 15815631]
14. Harper J; Skerry C; Davis SL; Tasneen R; Weir M; Kramnik I; Bishai WR; Pomper MG; Nuermberger EL; Jain SK, Mouse Model of Necrotic Tuberculosis Granulomas Develops Hypoxic Lesions. Journal of Infectious Diseases 2012, 205 (4), 595–602. [PubMed: 22198962]
15. Ordonez AA; Tasneen R; Pokkali S; Xu Z; Converse PJ; Klunk MH; Mollura DJ; Nuermberger EL; Jain SK, Mouse model of pulmonary cavitary tuberculosis and expression of matrix metalloproteinase-9. Disease models & mechanisms 2016, 9 (7), 779–788. [PubMed: 27482816]

16. Van Heeswijk R; Dannemann B; Hoetelmans R, Bedaquiline: a review of human pharmacokinetics and drug–drug interactions. Journal of Antimicrobial Chemotherapy 2014, 69 (9), 2310–2318. [PubMed: 24860154]

17. Zhou D; Chu W; Voller T; Katzenellenbogen JA, Copper-Mediated Nucleophilic Radiobromination of Aryl Boron Precursors: Convenient Preparation of a Radiobrominated PARP-1 Inhibitor. Tetrahedron Lett 2018, 59 (20), 1963–1967. [PubMed: 30349147]

18. Reilly SW; Makvandi M; Xu K; Mach RH, Rapid Cu-Catalyzed [(211)At]Astatination and [(125)I]Iodination of Boronic Esters at Room Temperature. Org Lett 2018, 20 (7), 1752–1755. [PubMed: 29561158]

19. Taylor NJ; Emer E; Preshlock S; Schedler M; Tredwell M; Verhoog S; Mercier J; Genicot C; Gouverneur V, Derisking the Cu-Mediated (18)F-Fluorination of Heterocyclic Positron Emission Tomography Radioligands. J Am Chem Soc 2017, 139 (24), 8267–8276. [PubMed: 28548849]

20. Lenaerts A; Barry CE 3rd; Dartois V, Heterogeneity in tuberculosis pathology, microenvironments and therapeutic responses. Immunol Rev 2015, 264 (1), 288–307. [PubMed: 25703567]

21. McLeay SC; Vis P; van Heeswijk RP; Green B, Population pharmacokinetics of bedaquiline (TMC207), a novel antituberculosis drug. Antimicrob Agents Chemother 2014, 58 (9), 5315–24. [PubMed: 24957842]

22. Aboagye EO; Price PM; Jones T, In vivo pharmacokinetics and pharmacodynamics in drug development using positron-emission tomography. Drug Discov Today 2001, 6 (6), 293–302. [PubMed: 11257581]

23. Jain SK; Ordonez A; Kinikar A; Gupte N; Thakar M; Mave V; Jubulis J; Dharmshale S; Desai S; Hatolkar S; Kagal A; Lalvani A; Gupta A; Bharadwaj R, Pediatric tuberculosis in young children in India: a prospective study. Biomed Res Int 2013, 2013, 783698. [PubMed: 24386640]

24. Be NA; Kim KS; Bishai WR; Jain SK, Pathogenesis of central nervous system tuberculosis. Curr Mol Med 2009, 9 (2), 94–9. [PubMed: 19275620]

25. Wilkinson RJ; Rohlwink U; Misra UK; van Crevel R; Mai NTH; Dooley KE; Caws M; Figaji A; Savic R; Solomons R; Thwaites GE; Tuberculous Meningitis International Research, C., Tuberculous meningitis. Nat Rev Neurol 2017, 13 (10), 581–598. [PubMed: 28884751]

26. Jain SK; Tobin DM; Tucker EW; Venketaraman V; Ordonez AA; Jayashankar L; Siddiqi OK; Hammoud DA; Prasadarao NV; Sandor M; Hafner R; Fabry Z; Group NIHTMW, Tuberculous meningitis: a roadmap for advancing basic and translational research. Nat Immunol 2018, 19 (6), 521–525. [PubMed: 29777209]

27. Akkerman OW; Odish OF; Bolhuis MS; de Lange WC; Kremer HP; Luijckx GJ; van der Werf TS; Alffenaar JW, Pharmacokinetics of Bedaquiline in Cerebrospinal Fluid and Serum in Multidrug-Resistant Tuberculous Meningitis. Clin Infect Dis 2016, 62 (4), 523–4. [PubMed: 26534926]

28. Rohlwink UK; Mauff K; Wilkinson KA; Enslin N; Wegoye E; Wilkinson RJ; Figaji AA, Biomarkers of Cerebral Injury and Inflammation in Pediatric Tuberculous Meningitis. Clin Infect Dis 2017, 65 (8), 1298–1307. [PubMed: 28605426]

29. Kuhar M; Yamamura HI, Localization of cholinergic muscarinic receptors in rat brain by light microscopic radioautography. Brain Res 1976, 110 (2), 229–43. [PubMed: 938940]

30. Weinstein E; Liu L; Ordonez A; Wang H; Hooker JM; Tonge P; Jain S, Noninvasive determination of 2-[18F]-fluoroisonicotinic acid hydrazide pharmacokinetics by positron emission tomography in Mycobacterium tuberculosis-infected mice. Antimicrobial agents and chemotherapy 2012, 56 (12), 6284–6290. [PubMed: 23006755]

31. O'Connell KE; Mikkola AM; Stepanek AM; Vernet A; Hall CD; Sun CC; Yildirim E; Staropoli JF; Lee JT; Brown DE, Practical murine hematopathology: a comparative review and implications for research. Comparative medicine 2015, 65 (2), 96–113. [PubMed: 25926395]

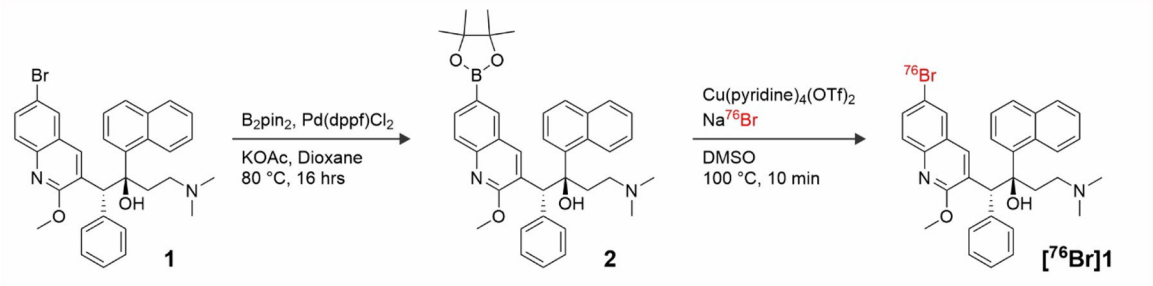

Figure 1.
Synthesis of boronic ester precursor **2** and radiosynthesis of ^{76}Br-bedaquiline

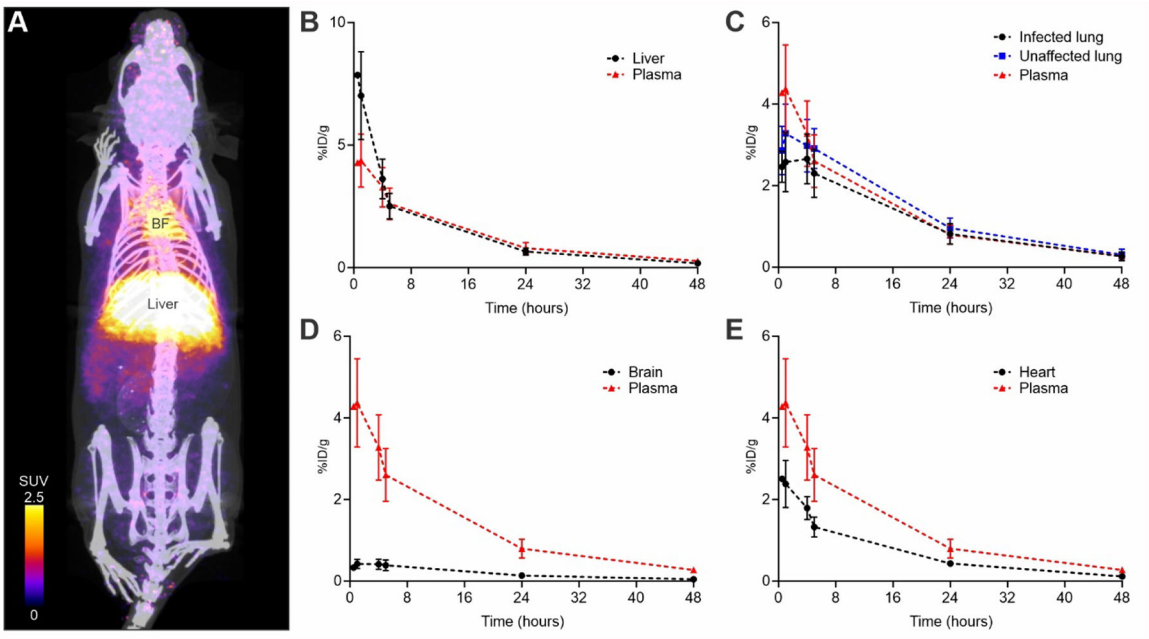

Figure 2. ^{76}Br-Bedaquiline PET of *M. tuberculosis*-infected mice.

(**A**) Three-dimensional maximum intensity projection of ^{76}Br-bedaquiline PET/CT of a representative mouse, one hour after tracer-injection. ^{76}Br-Bedaquiline localizes rapidly to the liver and the adipose-rich brown fat (BF). Time-activity curves in plasma and liver (**B**) lung (**C**), brain (**D**) and heart (myocardium) (**E**). Data represented as mean ± standard deviation, n=3 animals.

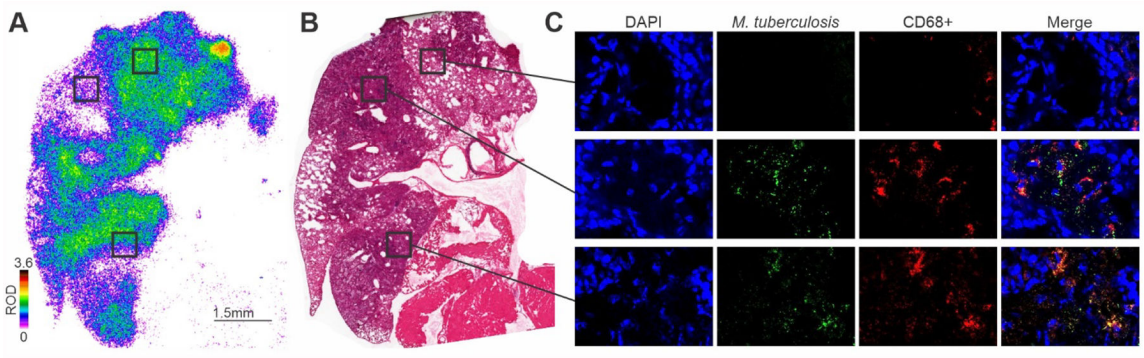

Figure 3. High-resolution 2D-Autoradiography of ^{76}Br-Bedaquiline.

(**A**) Detailed, intralesional biodistribution of ^{76}Br-bedaquiline in lung tissues of an *M. tuberculosis*-infected mouse 6 hours after a single dose. Data represented as relative optical density (ROD). (**B**) Hematoxylin and eosin staining of the same lung section. (**C**) Immunofluorescence staining of the same tissue section (used for autoradiography). Cellular nuclei (DAPI), *M. tuberculosis*, CD68+ macrophages and merged images (magnification of 63×).